atmosphere

MDPI

Article

Urban Spatial Patterns and Heat Exposure in the Mediterranean City of Tel Aviv

Moshe Mandelmilch [1], Michal Ferenz [1], Noa Mandelmilch [1] and Oded Potchter [2,*]

1 Department of Geography and Human Environment, Porter School of the Environment and Earth Sciences, Faculty of Exact Science, Tel Aviv University, Tel Aviv 699780, Israel; mandelmilch@mail.tau.ac.il (M.M.); Michalferenz@mail.tau.ac.il (M.F.); mandelmilch1@mail.tau.ac.il (N.M.)

2 Department of Geography, Beit Berl College, Beit Berl 44905, Israel

* Correspondence: potchter@tauex.tau.ac.il; Tel.: +972-528355480

Received: 30 July 2020; Accepted: 8 September 2020; Published: 10 September 2020

check for updates

Abstract: This study aims to examine the effect of urban spatial patterns on heat exposure in the city of Tel Aviv using multiple methodologies, Local Climate Zones (LCZ), meteorological measurements, and remote sensing. A Local Climate Zone map of Tel Aviv was created using Geographic Information System (GIS), and satellite images were used to identify the spatial patterns of the urban heat island (UHI). Climatic variables were measured by fixed meteorological stations and by mobile cross-section. Surface and wall temperatures were obtained by satellite images and a hand-held infrared camera. Meteorological measurements at a height of 2 m showed that during midday the city is ~3.6 °C warmer than the surrounding rural area. The cooling effect of parks was evident only during the hot hours of the day (9:00–17:00). Land Surface Temperature in the southern part of the city was hotter by ~7–9 °C compared to the northern part due to lack of urban vegetation. Hot spots were found in compact midrise forms (LCZ 2) that are not ideal from the climatological perspective. Whereas compact low-rise forms (LCZ 3) were less heat vulnerable. The results of this study suggest that climatologists can provide planners and architects with scientific insight into the causes of and solutions for urban climatic heat exposure.

Keywords: Urban Heat Island (UHI); Local Climatic Zone (LCZ); Land Surface Temperature; urban geometry; heat stress

1. Introduction

Urban populations are exposed to an increasing frequency and intensity of weather extremes due to both regional and global climate changes and urban climate alteration, which tend to be exacerbated during the summer months [1,2]. The urban climate is characterized by an amplification of air temperature, a lowering of air humidity, and moderation of wind velocity [3,4]. Amplification of temperature can be observed in different layers, Surface Urban Heat Island (SUHI), and Urban Heat Island (UHI) related to air temperature of the canopy layer [5].

One of the most important implications of the UHI is the increase in heat stress during the day in the summer, which aggravates human discomfort [6–8]. Coping with the impact of the UHI on heat stress as well as on heat storage in buildings and on surfaces, building energy consumption, air quality, and human wellbeing, and understanding urban heat exposure of different urban morphology and pattern, motivates policymakers to find solutions for heat mitigation in order to build climate resilient cities [3,4,9,10].

Land use change caused by urbanization is the primary driving factor of UHI in various cities around the world [11]. For example, in Berlin, a simulation of longitudinal variations of both temperature and land surface temperature show good agreement with urban fraction [12]. In Bucharest, day and night UHI intensity was higher in industrial zones than in forests and water bodies [13]. A similar finding was found in the Yangtze river area in China, where the average temperature of the built-up area was higher than the green areas in summer during the day by 3 °C and at night by about 2 °C [14].

The climate of urban areas exhibits spatial thermal differences within the urban setting and between urban and rural environments [15] due to diverse urban morphology, materials, prevailing meteorological conditions, and pollutant emissions [16]. Hence, the challenge of urban climatologists is to identify, measure, and understand the local complexities of urban climatic components and their effect on heat stress variability [17]. The method of Local Climate Zone (LCZ) [17,18] provides a research framework for urban climate studies and allows intercomparisons between cities to be made. The LCZ method subdivides the urban area into 17 different units, 10 built-up areas, categorized as LCZ1 to 10 according to building density and building height, and 7 open spaces, categorized as A to G according to land cover characteristic and vegetation function cover. These sub-divisions can help classify urban temperature magnitude and intensity in relation to surface cover, building heights and building surface fraction (BSF), greenery, materials, and human activity.

The LCZ classification has become a methodological tool for the analysis of UHI and the causes of UHI intensity [5,19,20]. Thus, the LCZ classification scheme can be used as a basis for heat exposure analysis in the urban area [21,22]. Currently, the World Urban Database and Access Portal (WUDAPT) is the most widely used method for LCZ mapping of cities around the world. Most LCZ studies have been carried out in temperate and cold climates [23,24], while only a few studies of LCZ classification have been implemented in Mediterranean climate cities [24]. A brief review of LCZ studies shows that most of them employed satellite remote sensing (RS) and mobile measurement and a few studies used fixed meteorological station [5,23].

In-situ observation by fixed meteorological station or mobile measurements and [RS] observation are the common methods for UHI studies [25]. Each method has its advantages and disadvantages. A network of fixed meteorological stations measured consistently all daily hours but cannot accurately represent the spatial pattern of UHI due to their limited number [26]. Mobile measurements can measure the micro-environment but are restricted to several hours of the day [26]. RS can demonstrate UHI pattern but is constrained by low temporal resolution and cannot demonstrate climatic temporal variation [23,27].

Although the UHI phenomenon in Israeli cities had been previously studied by fixed meteorological stations, mobile measurements, and RS, e.g., Tel Aviv [28,29], Eilat [30], and Beer Sheva [31–33], the UHI had not been investigated using the LCZ method in any Israeli cities.

The aims of the study were: (1) to examine the intensity and dynamics of the urban heat island in selected neighborhoods in Tel Aviv, (2) to determine the factors that can mitigate urban warming using multiple methods, data integration, meteorological measurements, remote sensing, and GIS analysis, (3) to suggest which LCZ is efficient for UHI mitigation in hot and humid cities, and (4) to assess the heat exposure of different LCZs and urban tissues to heat stress.

2. Methods, Tools, and Measurements

2.1. Study Area

The city of Tel Aviv is located at 32°06′ N 34°47′ E along the east coast of the Mediterranean Sea. The city area is 50 km^2 and spreads 14 km along the seashore with a width of 3 ± 6 km and a population of 451,523 inhabitants. The city of Tel Aviv is the center of the largest metropolitan area in Israel with a combined population of 3,985,000 [34]. The research area is the municipality of Tel Aviv, which is considered to be the heart of the metropolitan area.

Tel Aviv has a subtropical Mediterranean climate, Csa according to Koppen classification [35], and the rainy season is the winter. The city experiences hot and humid weather conditions during the summer. The summer is characterized by stable weather conditions, clear skies with minor changes from day to day. Based on Meteorological long-term data between 1995 and 2009 that were taken from Tel Aviv airport (Sde Dov meteorological station), located at the northern part of the city, 0.5 km from the coast line, the daily average maximum temperatures reach up to 30.6 °C and daily average minimum relative humidity is around 61%. Daily minimum temperatures are around 25.0 °C and daily average maximum relative humidity is around 83%. The wind regime is influenced by the Mediterranean Sea breeze, which blows during the day from the west and northwest, whereas during the night, it is affected by a light land breeze, which blows from the east and southeast [36]. In the summer, the city suffers from heat stress most of the day hours. Note that these climatic variables represent the seashore without the thermal effect of the urban built-up area. The city of Tel Aviv develops an UHI during the summer at both midday and at night [28].

2.2. Methodological Approach

The methodological approach of this study is an investigation from the general (meso-scale) to the specific (micro-scale) and an integrative one and includes four methods; (1) producing an LCZ map for the city of Tel Aviv. (2) RS monitoring of Tel Aviv's UHI (3) meteorological monitoring of heat vulnerable neighborhoods, and (4) an assessment of human thermal sensation to determine the heat stress exposure of different urban tissues of Tel Aviv.

2.2.1. Producing LCZ Map of the City

The LCZ map of Tel Aviv was produced using the three-step process suggested by Stewart and Oke (2012). In the first phase, Google street view images were used to characterize the different Tel Aviv climate zones in terms of: land uses, urban morphology, and urban geometry. In the second phase, based on these images, the climate zones were drawn using ARC MAP 10.6 software (ESRI Inc., Redlands, CA, USA). In the third phase, characteristics of local climate zones were calculated: Building Surface Fraction (BSF) were drawn using the Tel Aviv municipality's GIS website [37], and Height to Width ratio (H/W) and Sky View Factor (SVF), using a Nikon Camera model Coolpix 4300 with fish eye lens FC-E8, were identified for each LCZ. Finally, the map was validated by a field survey, in which RGB images of the streets were taken using a digital camera.

2.2.2. RS Monitoring of SUHI

In order to identify the spatial pattern of Tel Aviv's SUHI, Landsat 8 images from the summer months (June, July, and August) from the previous four years (2016–2019) were used (https://earthexplorer.usgs.gov/). A dataset of 18 reliable images (cloud coverage less than 3%) of the city was acquired. Band number 10 was used (10.60–11.19 μm), with a spatial resolution of 30 m. The information for the acquired images including meteorological data (air temperature and wind speed) were taken from the Tel Aviv Coastal Station (operated by the Israel Meteorological Service) and can be found in Table 1. Based on this dataset, a mean Land Surface Temperature (LST) map for the summer months (June–August) was produced.

Table 1. Information about the acquired Landsat 8 images including meteorological data: air temperature and wind speed (from the IMS Tel Aviv Coastal Station).

Date	Hour (Local Time)	Air Temperature (°C)	Wind Speed (m/s)
10 June 2016	11:10	25.7	5.5
26 June 2016	11:10	28.7	4.7
12 July 2016	11:11	28.9	4.5
28 July 2016	11:11	28.9	4
13 August 2016	11:11	29.1	4
13 June 2017	11:10	26.1	3.5
29 June 2017	11:10	28.7	4.5
15 July 2017	11:10	29.6	4.5
31 July 2017	11:11	29.9	4
7 June 2018	11:10	26.9	6.5
16 June 2018	11:10	30.3	2.5
2 July 2018	11:10	28.2	5
18 July 2018	11:10	29.2	6.5
3 June 2019	11:10	25.8	3.9
19 June 2019	11:10	28	3.1
5 July 2019	11:11	27.9	4.1
13 August 2019	11:10	29.9	3.3
22 August 2019	11:10	30	2.7

The brightness temperature (BT) was calculated from the thermal images of Landsat 8 (Table 1) based on Equations (1) and (2). Equation (1) presents the radiometric calibration of the images from Digital Numbers (DN) to radiance values, while Equation (2) presents the transformation of the radiance values into BT (in Kelvin) [38], which were converted to Celsius. The calculation was done in the ENVI image-processing package (ENVI, Boulder, CO, USA).

$$L_{\lambda} = \mathrm{M_L Q_{cal}} + \mathrm{A_L} \tag{1}$$

where L_{λ}= Top Of Atmosphere (TOA) radiance (Watts/(m^2 * srad *µm)); M_L = Band-specific multiplicative rescaling factor from the metadata; A_L = Band-specific additive rescaling factor from the metadata; Q_{cal} = Quantized and calibrated standard product pixel values (DN).

$$T = \frac{K_2}{ln\left(\frac{K_1}{L_{\lambda}} + 1\right)} \tag{2}$$

where T = At-satellite brightness temperature (K); L_{λ} = TOA spectral radiance (Watts/(m^2 * srad *mm)); K_1 = Band-specific thermal conversion constant from the metadata and $K_{2,}$ Band-specific thermal conversion constant from the metadata.

The BT is not necessarily the real Land Surface Temperature (LST) due to the emissivity parameter. Emissivity is defined as the ratio between the radiation emission of the object relative to the radiation emission of a "true black body" (emissivity value of 1). Every material in the urban area has its own emissivity value, determined by its thermal properties. This study focuses on the patterns of the SUHI and assumes that the BT is close to the real LST because the majority of urban objects and surfaces (e.g., asphalt and vegetation) have emissivity values close to 1. This principle was introduced by Sabins [39] and applied in recent SUHI studies in Tel Aviv [40] and Beer Sheva [33].

In addition, a Normalized Difference Vegetation Index (NDVI) for the entire city area was calculated based on Landsat 8 images from June 2019 (pixel size of 30 m). The raw data were converted into radiance values based on Equation (1) and then transformed into reflectance values based on an Internal Average Relative Reflectance (IAAR) algorithm. This process was done in the ENVI image-processing package (ENVI, Boulder, CO, USA). Afterward, the NDVI values were calculated using Equation (3) using the ENVI image-processing package (ENVI, Boulder, CO, USA).

$$\mathrm{NDVI} = (\mathrm{R}_{0.87} - \mathrm{R}_{0.66})/(\mathrm{R}_{0.87} + \mathrm{R}_{0.66}) \tag{3}$$

where R is the reflectance values in a certain spectral band (μm). Band 5 (0.87 μm) and band 4 (0.66 μm) were used.

2.2.3. Meteorological Monitoring

After identification of the spatial pattern of SUHI, two neighborhoods located in the hottest area of the city, the “Shapira neighborhood” and “Florentine neighborhood”, were chosen as a case study for a meteorological field survey (Figure 1). The meteorological field survey was conducted between 20–21 June, 2019 on the day of the summer solstice, under typical summer condition with clear skies. Two methods of meteorological monitoring were applied. Two Campbell Sci. automatic meteorological stations were situated in the “Shapira neighborhood” and two in the “Florentine neighborhood” (see Figure 1b). Within each neighborhood, one station was located in a N-S orientated street and the other in an E-W orientated street. An additional station was located in the rural area of Palmachim 1 km from the seashore. Air temperature and relative humidity were measured at a height of 2 m, and wind direction and wind velocity at a height of two meters. Readings were taken every second with the resulting data averaged and stored every 5 min using a Campbell Sci 21× data logger. Table 2 summarizes the measured meteorological variables, the instruments used for data collection, and their sensors’ accuracy. Two meteorological stations were used as reference stations, “Tel Aviv Coast station”, operated by the Israeli Meteorological Service, and “Hakfar Hayarok” Station, operated by the Ministry of the Environmental Protection. Radiation data were taken from the nearest Israeli Meteorological Service (IMS) station. Wind speed in all stations was measured at height of 2 m above ground, with exception of Tel Aviv coast station at which it was measured at heights of 10 m. Therefore, wind speed at this station was converted to 2 m above ground according to Equation (4) [41]:

$$\mathrm{V_h} = \mathrm{V_{10}} \times 0.233 + 0.656 \times \mathrm{LOG}(\mathrm{h} + 4.75) \tag{4}$$

where V is wind speed in a specific height and h is the desired height.

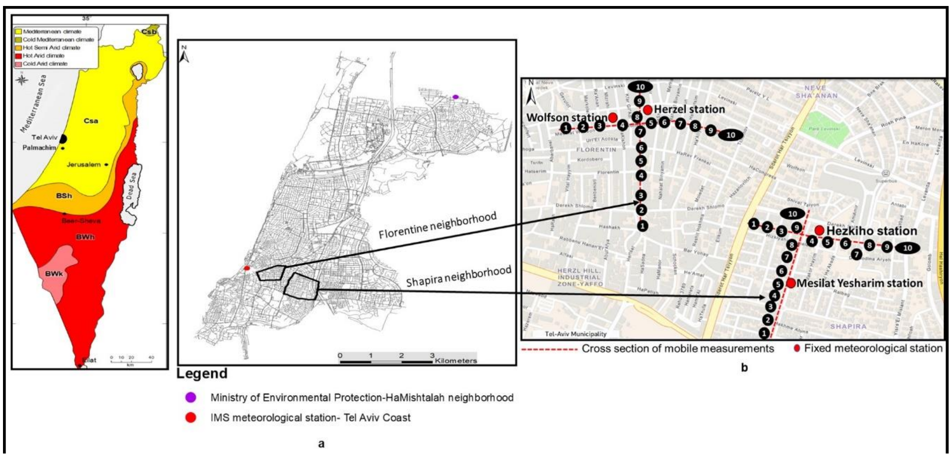

Figure 1. Study site location: (**a**) Map of Tel Aviv with the location of the investigated sites (**b**) Shapira Neighborhood and Florentine Neighborhood and the location of fixed meteorological stations and the location of cross-section of mobile measurements [37].

Table 2. Measured meteorological variables, instruments, and sensors' accuracy.

Variable	Unit	Instrument	Accuracy
Air temperature	°C	Campbell HMP45C-type	±0.2 °C
Relative humidity	%	Campbell HMP45C-type	±2%
Wind direction	Degree (°)	Young 05103 anemographs	3°
Wind speed	m/s	Young 05103 anemographs	±0.3 m/s

The second—mobile traverse measurements were conducted in each of the four selected streets every couple of hours. Each traverse included 10 points along the street (Figure 1b). Temperature, relative humidity, and wind speed measurements were taken using a Kestrel 3000 pocket weather meter. Reading in each point was taken in 1 s interval and were aggregated into 1 min average data. All measurements were taken in the shade to avoid influences of direct radiation. All measurements were taken on the east side of north-south streets and on the northern side of west-east streets.

On the whole, the study was based on 7 meteorological stations that represent several urban tissues of the Tel Aviv and one station of the rural area as follows:

- The "Shapira neighborhood", characterized by orthogonal street orientation from north to south (N-S) and east to west (E-W) with a mix of dense and low-rise buildings (1–3 stories). The land cover is mostly paved with few or no trees and it has a small urban garden in the center. A pair of streets was examined; Mesilat Yesharim St. (N-S) and Hizkiyahu St. (E-W) that contains a small neighborhood garden (5000 m^2) with irrigated lawn and mature Ficuse and Tipuana tipu trees in its eastern section.
- The "Florentine neighborhood" is characterized by orthogonal street orientation from north to south and east to west with a mix of dense and midrise buildings (3–9 stories). The streets hardly contain any trees or vegetation. A pair of streets was examined, Hertzl St. (N-S) and Wolfson St. (E-W) (Figure 1b).
- The "HaMishtalah neighborhood", located in the north-eastern part of the city, is characterized by mix of open and midrise buildings (3–9 stories) with green open spaces between the buildings. The meteorological data were taken from the meteorological station "Hakfar Hayrok", which operated by the Ministry of Environmental Protection. The station is located at the northern edge of the neighborhood and exposed to the sun most day hours.
- Tel Aviv seashore. The data for the Tel Aviv seashore was taken from the "Tel Aviv Coast station", the official meteorological station of the city that is operated by the Israeli Meteorological Service (IMS). The station is located 50 m from the seacoast, in LCZ 3800 m west of the Florentine neighborhood.
- The area of Palmachim served as a rural reference point. It is an open area of bare soil with bush and scrub tree cover. It is located at the edge of the metropolis area of Tel Aviv.

2.2.4. RS Monitoring of Local Hot Spots

A thermal image of Landsat 8 from 19 June 2019 was used to identify the hot and cold spots in the neighborhoods. The image was processed based on Equations (1) and (2) as described in Section 2.2.2. NDVI of the neighborhoods was calculated using Plant Scope image (pixel size of 3 m) from 19 June 2019 [42]. The NDVI was calculated on the reflectance image corrected by Planet [28] using Equation (5).

$$\mathrm{NDVI} = (\mathrm{R}_{820} - \mathrm{R}_{630})/(\mathrm{R}_{820} + \mathrm{R}_{630}) \quad (5)$$

where R is the reflectance values in a certain spectral band (nm). Band 4 (820 nm) and band 3 (630 nm) were used.

Thermal images of the street segments were acquired using a Fluke TI 300 pro hand-held IR camera that enables the observation of high-resolution IR information about the objects [43]. The images were taken at midday, in various locations throughout the neighborhood, allowing visualization of the thermal features of different objects such as: different vegetation types, buildings, walls, roofs, asphalt roads, pavements, and cars. Since different materials have different emissivity, the emissivity of certain objects in the images was corrected using SmartView software (Fluke Inc., Everett, WA, USA). The chosen objects were marked and then an appropriate emissivity estimate value was inserted manually based on the information presented in Sabins [39].

2.2.5. Thermal Sensation Calculation

Human thermal sensation was assessed using the physiological equivalent temperature (PET) based on the human energy balance [44], which is the most commonly used thermal index [45]. The PET has been used in numerous studies of urban built-up areas with complex terrain and shading patterns, where it generated accurate predictions of thermal environments [46,47]. The PET is officially recognized as a tool for human biometeorological evaluation of climate in urban and regional planning. The PET was calculated using the RayMan software [47,48]. The RayMan model, developed according to Guideline 3787 of the German Engineering Society (VDI, 1998), calculates the radiation flux in simple and complex environments on the basis of various parameters, such as air temperature, air humidity, wind velocity, degree of cloud cover, time of day and year, and the albedo of the surrounding surfaces' elevation and location. According to the model, the calculation of thermal sensation required adjustment of the following constants: body surface has been standardized to 1.9 m^2, which represents a human with a height of 1.75 m and a bodyweight of 75 kg [49,50]; the rate of metabolic energy transformation (work metabolism) based on 80 W for a standing person and the insulation factor of clothing (Icl) has been standardized to 0.9 for an indoor business suit [51].

3. Results

3.1. The LCZ Map of the City of Tel Aviv

The LCZ map of Tel Aviv clearly presents the urban structure of the city. In general, the southern part of the city, which is the oldest part, is denser, more compact, and contains areas with a high building fraction such as LCZ 2 (compact midrise) and LCZ 3 (compact low-rise) with few green open spaces (LCZ A and B). The northern and the northeastern part of the city is more modern and less dense and contains sparser LCZs, such as LCZ 4 (Open high-rise), LCZ 5 (open midrise), and LCZ 6 (open low-rise), and open LCZs, such as LCZs A, B, C, D, E, F, and G (Figure 2).

3.2. RS Monitoring of SUHI

A mean LST summer map (June-August) for the years 2016–2019 based on 18 images illustrates the spatial pattern of Tel Aviv's SUHI (Figure 3a). The amplitude of the LST varied from 27–41.1 °C. In general, there are differences between the LST in the northern and the southern part of the city. The southern part of the city is hotter by ~6–8 °C than the northern part (Figure 3a). It seems that a daily SUHI has developed mainly in the south part of the city. Note that the temporal resolution does not necessarily represent the maximum LST temperature since the images were acquired in the late morning and not in the peak hours (3–4 p.m.) (Table 1). The NDVI map of Tel Aviv, based on Landsat 8 images from June 2019 (Figure 3b), shows higher NDVI values in the northern part compared to the southern part, which reflects the higher levels of vegetation cover in the northern part of the city (e.g., urban gardens and parks, treed streets, and gardens between the buildings). Viewing the two images (LST and NDVI) illustrate that the hottest part of the city is characterized by lower NDVI values.

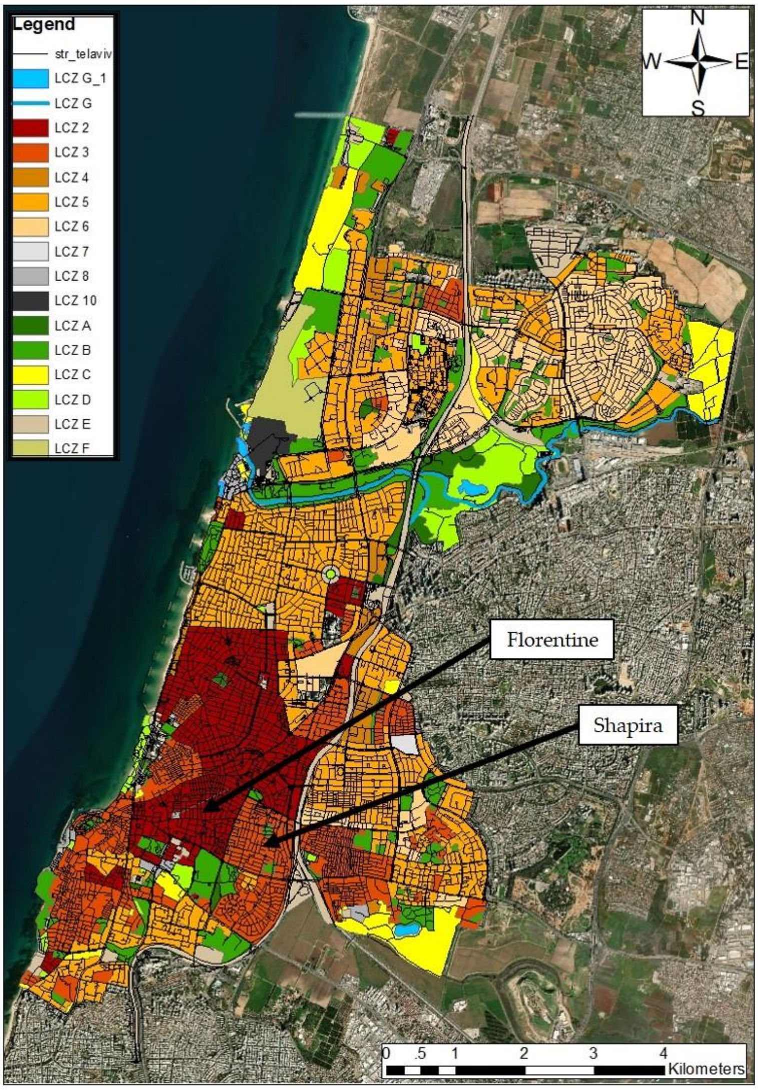

Figure 2. Local climatic map of Tel Aviv.

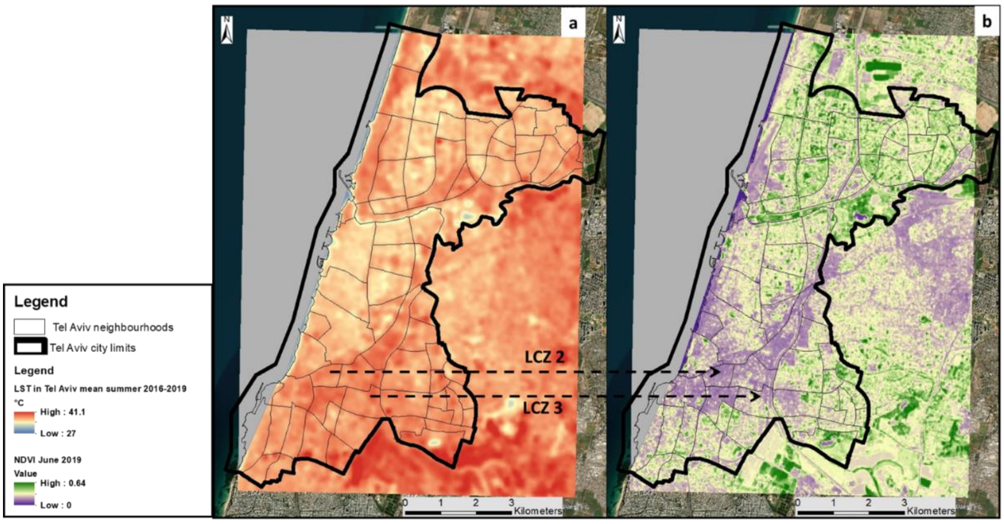

Figure 3. Landsat 8 images: (**a**) A mean land surface temperature (LST) summer 2016–2019 (June–August) map and (**b**) A mean normalized difference vegetation index (NDVI) from June 2019.

It seems that there is a strong relationship between the spatial pattern of Tel Aviv's SUHI and the LCZ map, the compact built LCZs of the city are warmer than the open built LCZs. Therefore, for further analysis of the heat exposure of the city of Tel Aviv, the study selected two neighborhoods in the southern part of the city: "Florentine neighborhood" and "Shapira neighborhood" (Figure 3). Although both neighborhoods are located in the hottest part of the city and are in close proximity to each other, they have different urban tissue. The "Florentine neighborhood" is classified as LCZ 2, with compact midrise buildings, 3–5 stories, with a BSF of ~65%, and hardly any trees along the streets. Two typical streets represent the neighborhood tissue; one, Hertzl St. running from north to south with an SVF of 0.23, and a H/W of 1.5, and the second, Wolfson St. running from East to West with an SVF of 0.35 and a H/W of 0.77. The "Shapira neighborhood" is classified as LCZ 3, with compact low-rise buildings, 1–3 stories, with a BSF of ~45%, and with some tress along the streets. Two typical streets represent the neighborhood tissue; one, Mesilat Yesharim St., running from north to south, has an SVF of 0.44 and a H/W of 0.35, and the second, Hizkiyahu St., running from east to west axis, has an SVF of 0.42 and a H/W of 0.51. Along this street, there is a small neighborhood garden covered with lawn and mature trees, which has an SVF of 0.1.

As a reference for the rural environment, climatic data were collected from two meteorological stations: the Tel Aviv Coast Station situated on the seafront, 800 m west of the Florentine neighborhood and the Palmachim Station located on the southern edge of the Tel Aviv metropolis, 1 km from the seashore and, classified as LCZ C due to the open terrain, low bushes, shrubs, and agricultural. As a result, the SVF equals to 0.9 (see Table 3).

Table 3. Values of geometric and surface cover properties for local climate zones of Tel Aviv.

LCZ	Site	Street Orientation	Photo on Ground Level	Aerial Photo	Fish Eye Photo	SVF BSF H/W
2	Florentine Neighborhood	East-West (Wolfson St.)		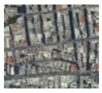		0.23 62.86% 1.5
2	Florentine Neighborhood	North-South (Hertzl St.)				0.35 65.40% 0.77
3	Shapira Neighborhood	North-South (Mesilat Yesharim St.)				0.44 40.42% 0.35
3	Shapira Neighborhood	East-West (Hizkiyahu St.)				0.42 45.79% 0.51
B	Neighborhood Garden (Shapira)	-				0.1 - 0
C	Palmachim	-		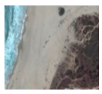		0.9 - 0

3.3. Meteorological Monitoring

Meteorological monitoring by fixed stations was conducted at "Florentine neighborhood", "Shapira neighborhood", "Tel Aviv Coast Station", and Palmachim rural area to demonstrate the intensity and dynamic of the Tel Aviv UHI (Figure 1). Figure 4 presents hourly temperatures, relative humidity, and wind speed for a continuous 24-h period between 20 and 21 June, 2019. The east-west oriented street (Wolfson St.) in the "Florentine neighborhood" was the hottest during the day and night. At midday, the Florentine neighborhood is hotter by ~3.6 °C than the rural area and Coast Station, and at dawn by 4 °C than the rural area and only 1 °C hotter than the Coast Station. The "HaMishtalah neighborhood" located at the northeastern of Tel Aviv was cooler by ~1–2 °C than the southern neighborhoods. In both southern neighborhoods, Shapira and Florentine, during most of the daytime hours, the east-west oriented streets were hotter than the north-south orientated streets by ~1 °C and during the night the differences were slightly lower, while before sunrise these differences increased by up to 2 °C (Figure 4a).

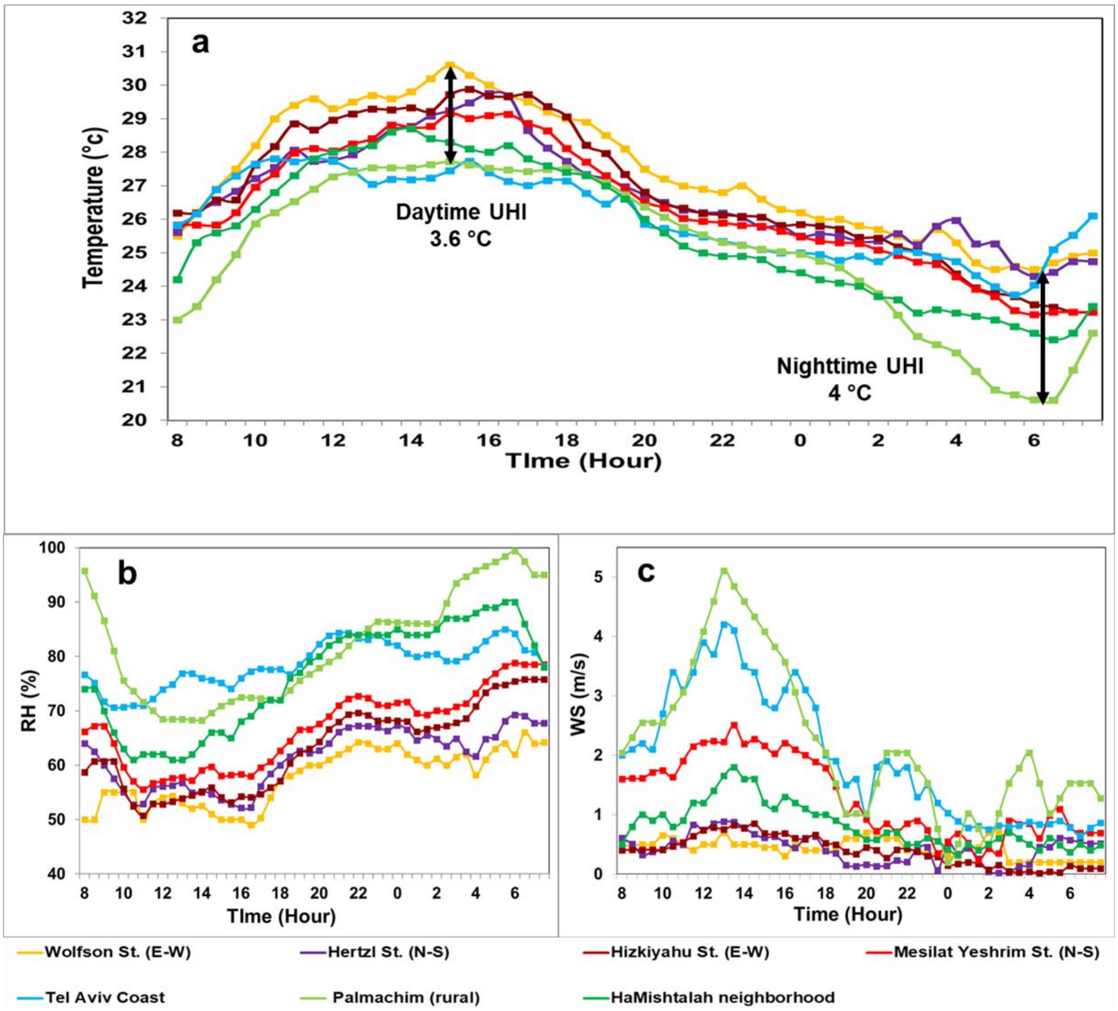

Figure 4. Meteorological monitoring in the selected streets of Shapira and Florentine neighborhoods during 20–21 of June, 2019: (**a**) Air temperature. (**b**) Relative humidity. (**c**) Wind speed.

At midday, the relative humidity values at the rural station were higher by 20–25% than at the city center and during the night by 35%. The relative humidity values along the north-south street were higher by ~5% than along the east-west street (Figure 4b).

During the hot hours of the day, when sea breeze reached its peak and blew towards the city, the wind velocity in the rural area and on the coast was significantly higher than in the built-up areas. At midday, wind velocity of 5 m/s was observed on the coast whereas, in the city, wind velocity was less than 2.5 m/s. At the night, the differences between the stations decreased (2 m/s in the open areas and less than 1 m/s in built-up areas (Figure 4c).

Mobile traverse measurements along each of the selected streets were carried out every two hours. The results demonstrate that temperatures along each street can vary from one point to another as a result of the immediate environment (Figure 5). In general, in both neighborhoods, the temperatures at the east-west streets were up to 1–2 °C warmer than north-south streets both day and night. In the north-south street, the temperature differences showed a slight increase from south to north during the day, indicating that the northern part of the neighborhoods is slightly warmer than the southern part. In the east-west street, the temperature differences showed a slight increase from east to west during the day, indicating that the west part of the neighborhood is slightly warmer than the eastern part. The notable finding in the east-west street cross-section (Hizkiyahu St.) in the Shapira neighborhood was the cooling effect caused by the neighborhood garden, which reduced temperatures by up to 3.5 °C. This cooling effect was more pronounced during the hot hours of the day while after sunset this effect vanished (see point 7, Figure 5a). It can be seen that the differences in PET °C values are more pronounced than those in air temperature °C vales alone (Figure 5a,b). During midday at 12:00, the PET values in all four streets were above 40 °C PET and defined as "very hot". The PET values for the E-W street of Florentine were the highest over 46 °C PET. At the E-W street in the Shapira neighborhood near the fixed station, PET values were 43.5 °C PET and reduced to 28 °C PET in the neighborhood garden a cooling effect of 15.5 °C PET. During nighttime the differences in temperature and in PET were negligible. These findings show that the east-west oriented street is warmer than the north-south oriented street with the same geometrical features and that the small neighborhood garden with irrigated lawn and mature trees has a significant heat-reducing effect during the day. Thus, in urban settings, the impact of vegetation on reducing heat stress in the daytime is more substantial than variations in urban geometry.

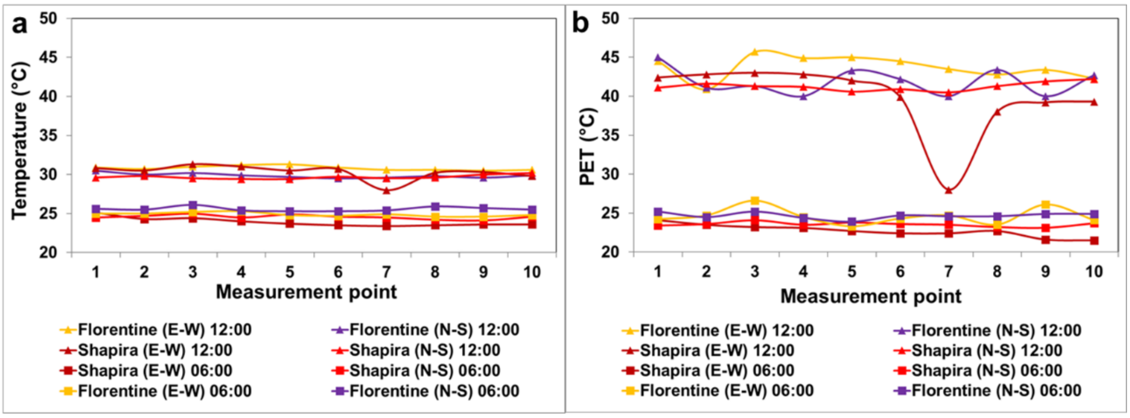

Figure 5. A comparison of (**a**) air temperature and (**b**) physiological equivalent temperature (PET) values along four street cross-sections in the Shapira and Florentine neighborhoods (Each line represents the variability of the air temperature and PET at a selected hour according to the measurement points) at 20 June 12:00 and at 21 June 06:00.

Hourly cross-sections along Hizkiyahu Street demonstrate the dynamic and intensity of the cooling effect of the Shapira neighborhood garden. The cross-section temperature measurements reveal that the neighborhood garden in the compact urban tissue can reduce temperature by up to 3.5 °C. This cooling is very pronounced during the late morning and midday and declines towards sunset, and is negligible during the nighttime (Figure 6).

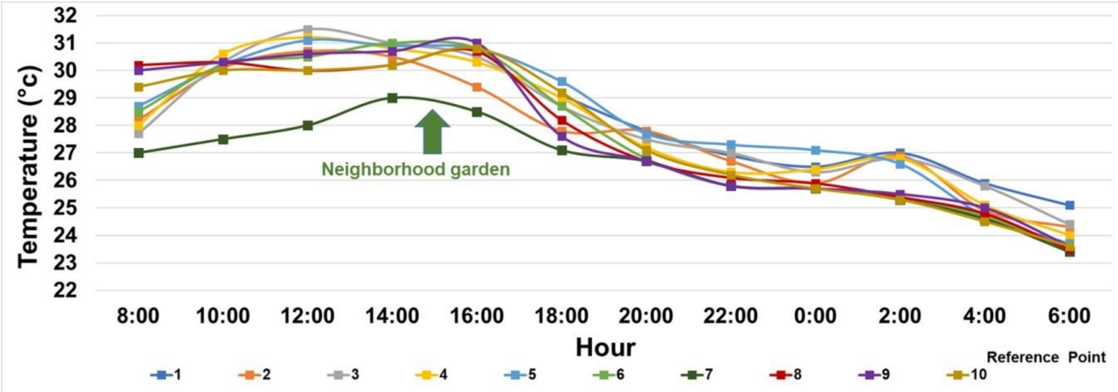

Figure 6. An hourly cross-section at 20–21 June, 2019, according to measuring points in Hizkiyahu St. (every line displays the temperature at a selected point around the clock). Line 7 (dark green) represents the neighborhood garden.

3.4. RS Monitoring of Local Hot Spots

Following the RS monitoring of Tel Aviv's LST and identification of the Tel Aviv summer SUHI on a meso-scale, this section analyses the local hot spots on a micro-scale. A thermal image of the Shapira and Florentine neighborhoods was acquired using Landsat 8 and NDVI image using the Plant Scope image (pixel size of 3 m) from 19.06.2019 [41]. In addition, thermal images of street segments (e.g., vegetation types, walls of buildings, roofs, asphalt roads, pavements, and vehicles), were acquired using a Fluke TI 300 pro hand-held IR Camera (Figure 7a,b).

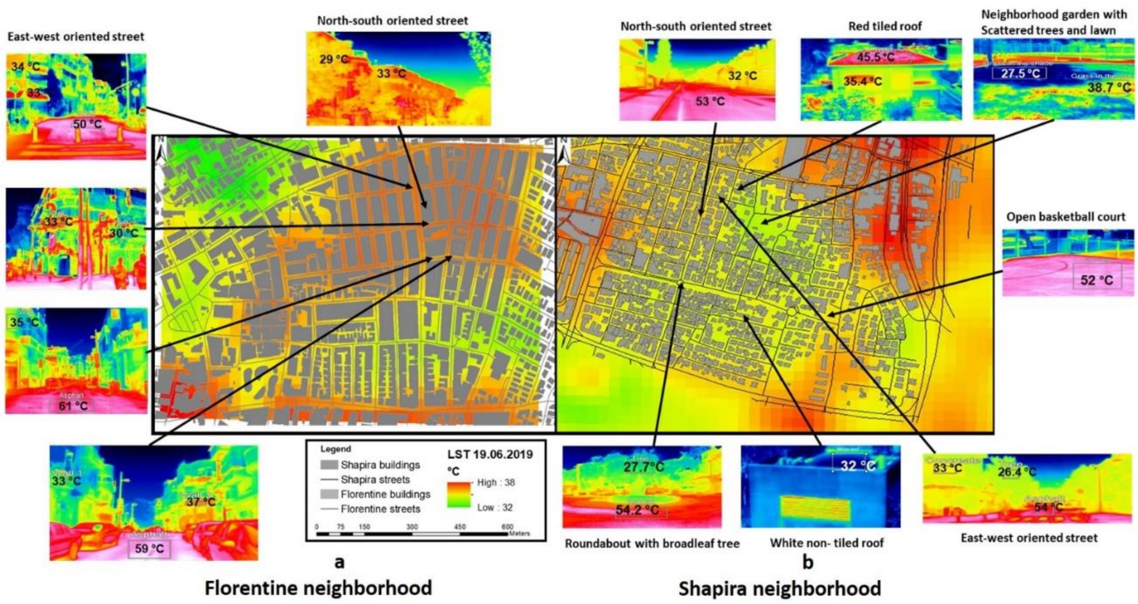

Figure 7. Thermal analysis in the neighborhoods. (**a**) Florentine neighborhood and (**b**) Shapira neighborhood. The base map is a Landsat 8 thermal image from19 June 2019.

In terms of LST, the Florentine neighborhood is hotter by ~2 °C than the Shapira neighborhood (Figure 7) due to three main reasons: (1) roof colors in Florentine are generally darker than in the Shapira neighborhood, (2) the streets in Florentine are wider than in the Shapira neighborhood and absorb more direct radiation, and (3) lack of urban vegetation cover in the Florentine neighborhood, as can be seen in the NDVI image (Figure 8). The inner LST pattern differs between the two neighborhoods; the northern part of the Florentine neighborhood is hotter than the southern part due to its higher building density and height. In the Shapira neighborhood, the western-northern part is hotter than the southern-eastern part due to differences in roof colors and lack of urban vegetation as demonstrated in the NDVI image (Figures 7b and 8b). In the western-northern part, most of the roofs are red-tiled roofs, while in the southern-eastern section most of the roofs are white non-tiled. Thermal images that were acquired using a hand-held IR camera revealed that the red-tiled roof temperature reached up to 45.5 °C, while at the same time, white, non-tiled roofs reached only 32.2 °C (Figure 7b).

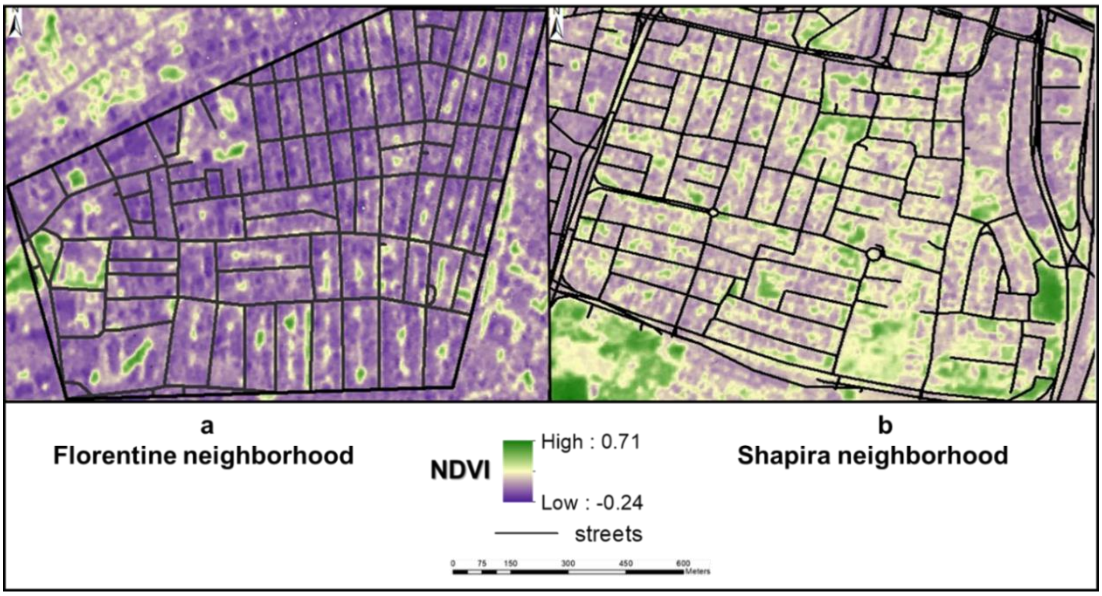

Figure 8. NDVI analysis of the neighborhoods based on Planet Scope images from 19 June 2019: (**a**) Florentine neighborhood and (**b**) Shapira neighborhood.

LST in the Shapira neighborhood demonstrated two LST patterns: first—the urban garden (Shapira garden) was cooler by ~6 °C than the dense built-up area at the western part of the neighborhood. Second—the LST southwest to the neighborhood was found to be ~2 °C cooler than the built-up area, due to a small urban forest with broadleaf trees (Figure 7b). Thermal images of the hand-held IR camera in the neighborhood garden distinguished between shaded grass and non-shaded grass in terms of LST. The non-shaded grass reached 38.7 °C, while grass under trees reached only 27.5 °C. The LST of the shaded grass can be identified only by the IR camera since satellite images capture only the canopy layer of the vegetation (Figure 7b).

Images of the hand-held IR camera revealed that in the Shapira neighborhood the LST of the E-W orientated street is hotter than the N-S orientated street. The asphalt road in the N-S street was cooler than the E-W oriented street. An open basketball court in the southern part of the neighborhood reached a temperature of 52 °C at midday. In the Florentine neighborhood, the images of the hand-held IR camera found the same temperature differences between the N-S oriented street and the E-W oriented street at midday. The asphalt in E-W oriented streets in the Florentine neighborhood is hotter than the asphalt in E-W oriented street in the Shapira neighborhood since the street is wider. Furthermore, the wall temperatures along the street canyons in the Florentine neighborhood were hotter than those of Shapira neighborhood (Figure 7a,b).

3.5. Heat Exposure in the City

The final stage of this study was to quantify the heat exposure of Tel Aviv using the thermal sensation scale of the PET, which was modified to the Mediterranean climate of Tel Aviv [52]. Figure 9 demonstrates numbers of comfort and heat stress hours during the daily cycle from the 20-21 June 2019 in a hot area of Tel Aviv in comparison to the rural area. The rural area Palmachim experiences 9 h of warm conditions, 1 h of slightly warm, and 5 h of slightly cool conditions. At the Tel Aviv Coast station, the heat hours were similar, 9 h of warm conditions and 1 h of slightly warm conditions. At the

HaMishtalah neighborhood, there were 4 h of slightly warm conditions and 7 h of hot condition (Note that the station was exposed to the sun most of the day hours). The most heat vulnerable site in the city was the E-W oriented street in the Florentine neighborhood, which experiences 21 h of heat stress, 9 h of very hot conditions, 5 h of hot conditions, and 7 h of slightly warm conditions. The E-W oriented street in the Shapira neighborhood experiences 11 h of heat stress, 9 h of very hot conditions, 1 h of hot conditions, and 1 h of slightly warm conditions. In Florentine, the N-S oriented street was less heat vulnerable with 3 h of very hot conditions, 3 h of hot, and 6 h of slightly warm conditions. In Shapira, there were 5 h of hot conditions, 2 h of warm conditions, and 1 h of slightly warm conditions.

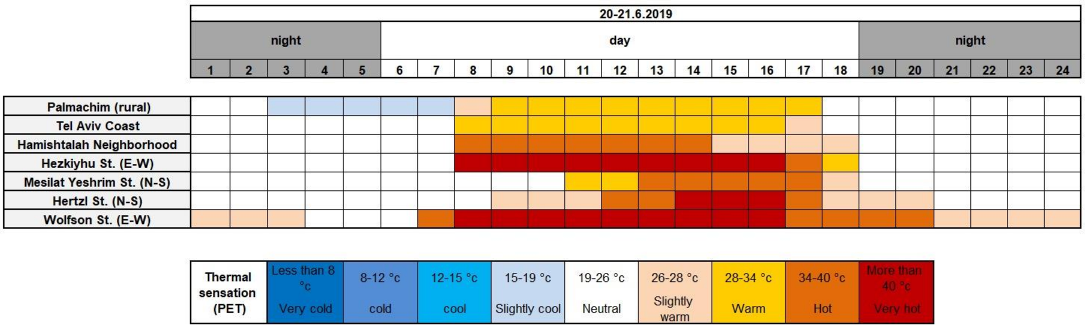

Figure 9. Hourly physiological equivalent temperature (PET) values in and around selected stations in Tel Aviv on20 June 2019.

4. Discussion

The aim of this study is to examine the intensity and dynamics of the heat exposure in Tel Aviv using multiple methods (Satellite RS, a network of fixed meteorological stations, mobile traverse measurements, a hand-held IR camera, and GIS analysis) in order to determine the parameters that influence urban warming. The integration of methods used in this study has allowed us to refine the findings of previous studies and quantify current UHI and urban heat exposure more accurately.

Previous studies that investigated Tel Aviv' UHI were based on a network meteorological of stations [28] or on Satellite RS [40,53,54]. Only one previous study, which investigated the UHI during the winter, used multiple methods of airborne RS, a network of fixed meteorological stations and mobile traverse measurements [29]. None of these studies used the LCZ method as a tool to analyze the UHI of Tel Aviv.

The main findings of this study are that the southern residential neighborhoods of Tel Aviv are the most heat vulnerable area of Tel Aviv. This is based on (1) A mean SUHI map based on 18 satellite images of the summer season that showed that the southern residential neighborhoods of Tel Aviv are ~6–8 °C hotter than the northern residential neighborhoods (2) A network of fixed meteorological stations measuring temperatures at street level (2 m above ground), which showed a daily summer UHI of 3.6 °C and a summer nighttime UHI of 4 °C. These results can be assessed as relabel since the summer season in Tel Aviv is characterized by stable weather conditions, clear sky with minor changes from day to day.

In addition, mobile measurements on a micro-scale were used in the hottest neighborhoods. The results showed that a neighborhood garden reduces air temperature by up to 3.5 °C and reduces heat stress up to 14 PET °C. Moreover, in the same urban tissue, E-W oriented streets are warmer than N-S oriented streets.

The notable findings of this study are that the city of Tel Aviv has developed a significant summer UHI and the southern residential neighborhoods of Tel Aviv are the most heat vulnerable area of the city. Furthermore, a neighborhood garden reduces air temperature and heat stress. Previous studies found that the magnitude of UHI was dependent on season and time of the day. The study of Bitan et al. [28] in Tel Aviv, which was based on a network of roof level stations, found a summer daily

UHI of 2 °C and a negligible UHI during the nighttime between the seashore and the city center and related it to the moderating effect of sea. The study of Saaroni et al. [29] focused on the winter season and found similar results of UHI based on roof level measurements. However, street level winter UHI was also observed during both day and nighttime and its magnitude were 4 °C and 5.6 °C, respectively. Satellite RS monitoring in 2015 showed that the LST of Tel Aviv's northern neighborhood is lower by 10 °C than industrial zones and the main central bus station located in the city center [39].

The UHI intensity in coastal cities may be affected by the land-sea interaction [55–57]. In the context of Tel Aviv, Bitan et al. [28] and Saaroni et al. [29] argued that the vicinity to the sea and sea breeze has a moderate effect on Tel Aviv's daily UHI. However, their studies were based on roof level net stations. The study of Balslev et al. [58] found that the effect of the sea breeze on thermal conditions during the summer at the street level in Tel Aviv is limited. Studies that have investigated the daily summer UHI in coastal Mediterranean cities point to the moderating effect of the sea breeze as measured on roof level [24,59,60]. However, the study of Salvati et al. [60] in Barcelona found a significant UHI intensity of 4.3 °C at street level, which is up to 2 °C higher than roof level UHI during the hottest hours of the day. A recent study in the coastal Mediterranean city of Bari, Italy, based on street level stations, found that the sea breeze can mitigate air temperature in coastal stations, but in stations located in LCZ 2 and 5, the sea breeze effect is weaker [61]. These findings support the results of our study that Tel Aviv has developed a significant summer UHI.

The significant finding of the present study is that there is an overlap between the spatial distribution of the SUHI and Local Climatic Zone map of Tel Aviv. Thus, there is a link between the morphological structure of the built-up area and the dynamic and intensity of the UHI of Tel Aviv. The compact residential neighborhoods, classified as LCZ 2 and 3, are the most heat vulnerable area. In the case of Tel Aviv, these neighborhoods (Shapira and Florentine) built in the early 20th century, are characterized by high-density buildings, as opposed to the more modern residential neighborhoods in the northern part of the city, which are classified as more open LCZ 5 and 6 and are distinguished by less dense buildings and more green open spaces [62].

The use of a multi-method for UHI studies can overcome the limitations of each specific method. For example, the spatial pattern of SUHI can be studied efficiently from satellite RS, however, the passing time of the satellite is restricted (in the case of Tel Aviv to 11:10 local time) and thus does not necessarily present the maximum LST temperature. On the other hand, the data collected from fixed meteorological station is consecutive and allows the identification of the peak and the minimum of the UHI and its daily dynamics.

The use of multi-method can provide a better understanding of the causes of the UHI. For example, the overlap of thermal image and NDVI maps shows clearly that urban areas that contain vegetation are less hot than dense urban areas with a lack of vegetation. In the case of Tel Aviv, the higher urban vegetation cover in the northern part of the city creates a moderating effect of ~8 °C on SUHI intensity.

The use of portable RS and meteorological measurements enables the identification of the impact of the immediate environment on urban warming on a micro-scale. The use of the hand-held IR-camera in this study allowed the thermal properties of different urban objects to be examined and their contribution to urban warming to be quantified. The results demonstrate that different types of land cover and land uses have a direct influence on the intensity and dynamics of the UHI. For example, the hand-held IR camera proves that in terms of vegetation cooling effect, broadleaf tree species are more efficient than lawns. It also demonstrates the thermal effect of different urban objects (e.g., roofs, walls of buildings, asphalt roads, vehicles, etc.), which absorb different amounts of direct solar radiation in correspondence with their thermal properties thus influencing the intensity and dynamics of the UHI. For instance, walls of buildings and asphalt roads in E-W oriented streets are hotter than N-S oriented streets since they are exposed to more hours of sun radiation. Another element that plays an important role on LST is the material and color of roofs since a tiled red roof can be 13 °C hotter than a flat white roof.

Finally, this study suggests that the use of multi-methods and data compilation allow heat exposure to be identified and quantified for localized urban areas. Data should be collected on three levels, satellite images on a macro-scale, fixed meteorological stations on a meso-scale, and mobile measurements and hand-held IR camera on a micro-scale. This integration of methods may lead to a more detailed image and holistic approach to the climatic analysis of the urban tissue.

5. Conclusions

This study analyzed the urban spatial patterns and heat exposure in the City of Tel Aviv using multiple methods (Satellite RS, a network of meteorological stations, mobile traverse measurements, a hand-held IR camera, and GIS analysis). The study showed that a Mediterranean city can develop a significant day and night UHI during the summer season. In the case of the urban spatial UHI patterns of Tel Aviv, it seems that the southern residential neighborhoods are the most heat vulnerable area as compared to other parts of the city during the summer season. Moreover, quantification of heat vulnerability in terms of a human thermal index can be higher than when expressed in air temperature values alone.

From mitigation of the urban heat island, the internal structure of the city plays an important role in determining the UHI spatial distribution. Neighborhood gardens and trees have the most significant effect on heat mitigation. They can reduce air temperatures by up to 3.5 °C. Street orientation is also an important element in heat mitigation. Air temperature in N-S orientated streets can be lower than up to 2 °C in comparison to E-W oriented streets in all types of LCZs. In terms of type of LCZ, air temperature in LCZ 2 (compact midrise) is warmer by ~1.5 °C than LCZ 3 (compact low-rise) and by ~2.5 °C than LCZ 5 (open midrise) and LCZ 6 (open low-rise).

The results of this study suggest that climatologists can provide planners and architects with data and insights for urban planning and rehabilitation in heat-vulnerable neighborhoods. In the case of the humid and hot climate of Tel Aviv, priority should be given to open LCZ types rather than compact ones, the urban tissue should contain neighborhood gardens with more shading trees and fewer lawns. In planning the urban street pattern, E-W oriented streets should be shaded where possible and prioritized for street greening to lower asphalt and pavement temperatures.

Author Contributions: M.M.; Remote sensing, field measurements, data visualization, software analysis, writing—original draft, M.F.; field measurements, data visualization, software analysis, data analysis, G.I.S. mapping, writing—original draft, N.M.; field measurements, data visualization, software analysis, G.I.S. mapping. O.P.; conceptualization, methodology, supervision, reviewing, editing. All authors have read and agreed to the published version of the manuscript.

Funding: This research was partly funded by the Center for Resilient Cities and Landscape of Colombia University, New York, and the municipality of Tel Aviv.

Acknowledgments: The authors wish to thank Johanna Lovecchio, Associate Director, and the team of the Center for Resilient Cities and Landscapes, Columbia University, New York, which supported this work as a part of Tet Aviv-Yafo Resilience Accelerator: Heat Vulnerability Analysis as a Tool for neighborhood-based action. The authors also wish to thank Beit Berl College for their contribution to this research. A special appreciation and thanks to students of Tel Aviv University and Beit Berl College for their active participation in the field measurements. The authors owe special thanks to the Tel Aviv Municipality and Omri Carmon, Deputy Chief Resilience Officer, for his assistance throughout the research stages. The authors would also like to thank Orli Ronen, Head of the Laboratory for Innovation and Sustainability in the city, the Porter School of Environmental Studies at Tel Aviv University.

Conflicts of Interest: The authors declare no conflict of interest.

References

1. Itzhak-Ben-Shalom, H.; Samuels, R.; Potchter, O.; Alpert, P. Recent trends and future predictions until 2060 of urban warming in four Israeli cities employing the RegCM climate model. *Am. J. Clim. Chang.* **2016**, *5*, 464–484. [CrossRef]
2. Potchter, O.; Ben-Shalom, H.I. Urban warming and global warming: Combined effect on thermal discomfort in the desert city of Beer Sheva, Israel. *J. Arid. Environ.* **2013**, *98*, 113–122. [CrossRef]

3. Landsberg, H.E. *The Urban Climate*; Academic Press: New York, NY, USA, 1981; pp. 231–235.
4. Oke, T.R. *Boundary Layer Climate*; Methuem Press: London, UK, 1987; pp. 288–297.
5. Bechtel, B.; Demuzere, M.; Mills, G.; Zhan, W.; Sismanidis, P.; Small, C.; Voogt, J. SUHI analysis using Local Climate Zones-A comparison of 50 cities. *Urban Clim.* **2019**, *28*, 100451. [CrossRef]
6. Baker, L.A.; Brazel, A.J.; Selover, N.; Martin, C.; McIntyre, N.; Steiner, F.R.; Musacchio, L. Urbanization and warming of Phoenix (Arizona, USA): Impacts, feedbacks and mitigation. *Urban Ecosyst.* **2002**, *6*, 183–203. [CrossRef]
7. Oleson, K.W.; Monaghan, A.; Wilhelmi, O.; Barlage, M.; Brunsell, N.; Feddema, J.; Steinhoff, D.F. Interactions between urbanization, heat stress, and climate change. *Clim. Chang.* **2015**, *129*, 525–541. [CrossRef]
8. Pantavou, K.; Theoharatos, G.; Mavrakis, A.; Santamouris, M. Evaluating thermal comfort conditions and health responses during an extremely hot summer in Athens. *Build. Environ.* **2011**, *46*, 339–344. [CrossRef]
9. Lim, J.; Skidmore, M. Heat Vulnerability and Heat Island Mitigation in the United States. *Atmosphere* **2020**, *11*, 558. [CrossRef]
10. Leal Filho, W.; Icaza, L.E.; Neht, A.; Klavins, M.; Morgan, E.A. Coping with the impacts of urban heat islands. A literature-based study on understanding urban heat vulnerability and the need for resilience in cities in a global climate change context. *J. Clean. Prod.* **2018**, *171*, 1140–1149. [CrossRef]
11. Li, H.; Zhou, Y.; Li, X.; Meng, L.; Wang, X.; Wu, S.; Sodoudi, S. A new method to quantify surface urban heat island intensity. *Sci. Total Environ.* **2018**, *624*, 262–272. [CrossRef]
12. Li, H.; Wolter, M.; Wang, X.; Sodoudi, S. Impact of land cover data on the simulation of urban heat island for Berlin using WRF coupled with bulk approach of Noah-LSM. *Theor. Appl. Climatol.* **2018**, *134*, 67–81. [CrossRef]
13. Cheval, S.; Dumitrescu, A. The summer surface urban heat island of Bucharest (Romania) retrieved from MODIS images. *Theor. Appl. Climatol.* **2015**, *121*, 631–640. [CrossRef]
14. Du, H.; Wang, D.; Wang, Y.; Zhao, X.; Qin, F.; Jiang, H.; Cai, Y. Influences of land cover types, meteorological conditions, anthropogenic heat and urban area on surface urban heat island in the Yangtze River Delta Urban Agglomeration. *Sci. Total Environ.* **2016**, *571*, 461–470. [CrossRef] [PubMed]
15. Grimmond, S. Urbanization and global environmental change: Local effects of urban warming. *Geogr. J.* **2007**, *173*, 83–88. [CrossRef]
16. Souch, C.; Grimmond, S. Applied climatology: Urban climate. *Prog. Phys. Geogr.* **2006**, *30*, 270–279. [CrossRef]
17. Kwok, Y.T.; Schoetter, R.; Lau, K.K.L.; Hidalgo, J.; Ren, C.; Pigeon, G.; Masson, V. How well does the local climate zone scheme discern the thermal environment of Toulouse (France)? An analysis using numerical simulation data. *Int. J. Climatol.* **2019**, *39*, 5292–5315. [CrossRef]
18. Stewart, I.D.; Oke, T.R. Local climate zones for urban temperature studies. *Bull. Am. Meteorol. Soc.* **2012**, *93*, 1879–1900. [CrossRef]
19. Middel, A.; Häb, K.; Brazel, A.J.; Martin, C.A.; Guhathakurta, S. Impact of urban form and design on mid-afternoon microclimate in Phoenix Local Climate Zones. *Landsc. Urban Plan.* **2014**, *122*, 16–28. [CrossRef]
20. Unger, J.; Lelovics, E.; Gál, T. Local Climate Zone mapping using GIS methods in Szeged. *Hung. Geogr. Bull.* **2014**, *63*, 29–41. [CrossRef]
21. Cai, Z.; Tang, Y.; Chen, K.; Han, G. Assessing the heat vulnerability of different local climate zones in the old areas of a Chinese megacity. *Sustainability* **2019**, *11*, 2032. [CrossRef]
22. Ochola, E.M.; Fakharizadehshirazi, E.; Adimo, A.O.; Mukundi, J.B.; Wesonga, J.M.; Sodoudi, S. Inter-local climate zone differentiation of land surface temperatures for Management of Urban Heat in Nairobi City, Kenya. *Urban Clim.* **2020**, *31*, 100540. [CrossRef]
23. Bechtel, B.; Alexander, P.J.; Beck, C.; Böhner, J.; Brousse, O.; Ching, J.; Demuzere, M.; Fonte, C.; Gál, T.; Hidalgo, J.; et al. Generating WUDAPT Level 0 data–Current status of production and evaluation. *Urban Clim.* **2019**, *27*, 24–45. [CrossRef]
24. Oliveira, A.; Lopes, A.; Niza, S. Local climate zones in five southern European cities: An improved GIS-based classification method based on Copernicus data. *Urban Clim.* **2020**, *33*, 100631. [CrossRef]
25. Mirzaei, P.A.; Haghighat, F. Approaches to study urban heat island–abilities and limitations. *Build. Environ.* **2010**, *45*, 2192–2201. [CrossRef]
26. Li, H.; Zhou, Y.; Wang, X.; Zhou, X.; Zhang, H.; Sodoudi, S. Quantifying urban heat island intensity and its physical mechanism using WRF/UCM. *Sci. Total Environ.* **2019**, *650*, 3110–3119. [CrossRef] [PubMed]
27. Wang, C.; Middel, A.; Myint, S.W.; Kaplan, S.; Brazel, A.J.; Lukasczyk, J. Assessing local climate zones in arid cities: The case of Phoenix, Arizona and Las Vegas, Nevada. *ISPRS J. Photogramm. Remot Sens.* **2018**, *141*, 59–71. [CrossRef]

28. Bitan, A.; Noy, L.; Turk, R. The impact of the seashore on the climate of Tel-Aviv. *Sci. Rep. Inst. Meteorol. Clim. Res. Karlsr. Univ.* **1992**, *16*, 147–160.
29. Saaroni, H.; Ben-Dor, E.; Bitan, A.; Potchter, O. Spatial distribution and microscale characteristics of the urban heat island in Tel-Aviv, Israel. *Landsc. Urban Plan.* **2000**, *48*, 1–18. [CrossRef]
30. Sofer, M.; Potchter, O. The urban heat island of a city in an arid zone: The case of Eilat, Israel. *Theor. Appl. Climatol.* **2006**, *85*, 81–88. [CrossRef]
31. Potchter, O.; Yaacov, Y.; Oren, G. The magnitude of the urban heat island of a city in an arid zone: The case of Beer Sheva, Israel. Proceeding of the 6th International Conference on Urban Climate, Gothenburg, Sweden, 12–16 July 2006; pp. 450–453.
32. Saaroni, H.; Ziv, B. Estimating the urban heat island contribution to urban and rural air temperature differences over complex terrain: Application to an arid city. *J. Appl. Meteorol. Climatol.* **2010**, *49*, 2159–2166. [CrossRef]
33. Zhou, B.; Kaplan, S.; Peeters, A.; Kloog, I.; Erell, E. "Surface,""satellite" or "simulation": Mapping intra-urban microclimate variability in a desert city. *Int. J. Climatol.* **2020**, *40*, 3099–3117. [CrossRef]
34. Central Bureau of Statistics. *1, Population and Density Per Sq. Km in Localities Numbering 5,000 Residents and More on 31*; Central Bureau of Statistics: Jerusalem, Israel, 2018; Volume 12.
35. Potchter, O.; Saaroni, H. An examination of the map of climatic regions of Israel according to the Koppen classification. *Stud. Geogr. Isr.* **1998**, *15*, 179–194.
36. Bitan, A.; Rubin, S. *Climatic Atlas of Israel for Physical and Environmental Planning and Design*; Ministry of Transport: Jerusalem, Israel, 1994.
37. Tel Aviv Municipality's GIS Website. Available online: https://gisn.tel-aviv.gov.il/iview2js4/index.aspx (accessed on 12 July 2020).
38. USGS. Retrieved from USGS. 2020. Available online: https://www.usgs.gov/land-resources/nli/landsat (accessed on 15 August 2020).
39. Sabins, F.F. *Remote Sensing: Principles and Applications*, 3rd ed.; Waveland Press: Long Grove, IL, USA, 2007.
40. Pelta, R.; Chudnovsky, A.A.; Schwartz, J. Spatio-temporal behavior of brightness temperature in Tel-Aviv and its application to air temperature monitoring. *Environ. Pollut.* **2016**, *208*, 153–160. [CrossRef] [PubMed]
41. Anon. *Observers' Handbook*; Meteorological Office: HMSO, UK, 1983.
42. Planet Application Program Interface: In Space for Life on Earth. San Francisco, CA. Available online: https://api.planet.com (accessed on 12 July 2020).
43. Chui, A.C.; Gittelson, A.; Sebastian, E.; Stamler, N.; Gaffin, S.R. Urban heat islands and cooler infrastructure–measuring near-surface temperatures with hand-held infrared cameras. *Urban Clim.* **2018**, *24*, 51–62. [CrossRef]
44. Höppe, P. The physiological equivalent temperature—A universal index for the biometeorological assessment of the thermal environment. *Int. J. Biometeorol.* **1999**, *43*, 71–75. [CrossRef] [PubMed]
45. Potchter, O.; Cohen, P.; Lin, T.P.; Matzarakis, A. Outdoor human thermal perception in various climates: A comprehensive review of approaches, methods and quantification. *Sci. Total Environ.* **2018**, *631*, 390–406. [CrossRef]
46. Matzarakis, A.; Rutz, F.; Mayer, H. Modelling radiation fluxes in simple and complex, environments e application of the RayMan model. *Int. J. Biometeorol.* **2007**, *51*, 323–334. [CrossRef]
47. Cohen, P.; Shashua-Bar, L.; Keller, R.; Gil-Ad, R.; Yaakov, Y.; Lukyanov, V.; Bar (Kutiel), P.; Tanny, J.; Cohen, S.; Potchter, O. Urban outdoor thermal perception in hot arid Beer Sheva, Israel: Methodological and gender aspects. *Build. Environ.* **2019**, *160*, 106–169. [CrossRef]
48. Matzarakis, A.; Rutz, F.; Mayer, H. Modelling radiation fluxes in simple and complex environments: Basics of the RayMan model. *Int. J. Biometeorol.* **2010**, *54*, 131–139. [CrossRef]
49. Mayer, H.; Höppe, P. Die Bedeutung des Waldes für die Erholung aus der Sicht der Humanbioklimatologie. *Forstwissenschaftliches Centralblatt* **1984**, *103*, 125–131. [CrossRef]
50. Mayer, H.; Höppe, P. Thermal comfort of man in different urban environments. *Theor. Appl. Climatol.* **1987**, *38*, 43–49. [CrossRef]
51. Jendritzky, G.; Menz, H.; Schirmer, H.; Schmidt-Kessen, W. *Methodik zur raumbezogenen Bewertung der thermischen Komponente im Bioklima des Menschen (Fortgeschriebenes Klima-Michel-Modell)*; Akademie fur Raumforschung und Landesplanung: Hannover, Germany, 1990; p. 114.
52. Cohen, P.; Potchter, O.; Matzarakis, A. Human thermal perception of Coastal Mediterranean outdoor urban environments. *Appl. Geogr.* **2013**, *37*, 1–10. [CrossRef]

53. Rotem-Mindali, O.; Michael, Y.; Helman, D.; Lensky, I.M. The role of local land-use on the urban heat island effect of Tel Aviv as assessed from satellite remote sensing. *Appl. Geogr.* **2015**, *56*, 145–153. [CrossRef]
54. Pelta, R.; Chudnovsky, A.A. Spatiotemporal estimation of air temperature patterns at the street level using high resolution satellite imagery. *Sci. Total Environ.* **2017**, *579*, 675–684. [CrossRef] [PubMed]
55. Freitas, E.D.; Rozoff, C.M.; Cotton, W.R.; Dias, P.L.S. Interactions of an urban heat island and sea-breeze circulations during winter over the metropolitan area of São Paulo, Brazil. *Bound. Layer Meteorol.* **2007**, *122*, 43–65. [CrossRef]
56. Ribeiro, F.N.; de Oliveira, A.P.; Soares, J.; de Miranda, R.M.; Barlage, M.; Chen, F. Effect of sea breeze propagation on the urban boundary layer of the metropolitan region of Sao Paulo, Brazil. *Atmos. Res.* **2018**, *214*, 174–188. [CrossRef]
57. Meir, T.; Orton, P.M.; Pullen, J.; Holt, T.; Thompson, W.T.; Arend, M.F. Forecasting the New York City urban heat island and sea breeze during extreme heat events. *Weather Forecast.* **2013**, *28*, 1460–1477. [CrossRef]
58. Balslev, Y.J.; Potchter, O.; Matzarakis, A. Climatic and thermal comfort analysis of the Tel-Aviv Geddes Plan: A historical perspective. *Build. Environ.* **2015**, *93*, 302–318. [CrossRef]
59. Moreno-Garcia, M.C. Intensity and form of the urban heat island in Barcelona. *Int. J. Climatol.* **1994**, *14*, 705–710. [CrossRef]
60. Salvati, A.; Roura, H.C.; Cecere, C. Assessing the urban heat island and its energy impact on residential buildings in Mediterranean climate: Barcelona case study. *Energy Build.* **2017**, *146*, 38–54. [CrossRef]
61. Martinelli, A.; Kolokotsa, D.D.; Fiorito, F. Urban Heat Island in Mediterranean Coastal Cities: The Case of Bari (Italy). *Climate* **2020**, *8*, 79. [CrossRef]
62. Resilience Accelerator Tel Aviv-Yafo|Urban Heat, Equity, Resilience, and the Future of the Public Realm. Available online: https://www.arcgis.com/apps/Cascade/index.html?appid=f713e4bb103f461da55f4cdf33648b00 (accessed on 12 July 2020).